GT2022-83029

A STUDY ON FUNDAMENTAL COMBUSTION PROPERTIES OF TRIMETHYL ORTHOFORMATE: EXPERIMENTS AND MODELING

John Mbũrũ Ngũgĩ*, Sandra Richter, Marina Braun-Unkhoff,

Clemens Naumann, Uwe Riedel[1]

German Aerospace Center (DLR)

Institute of Combustion Technology

Pfaffenwaldring 38-40, 70569 Stuttgart, Germany

[1] German Aerospace Center (DLR)

Institute of Low-Carbon Industrial Processes

Walther-Pauer-Straße 5, 03046 Cottbus, Germany

*Email: john.mburu@dlr.de

ABSTRACT

Trimethyl orthoformate (TMOF: $HC(OCH_3)_3$) has recently been examined as a viable biofuel. TMOF is a branched isomer of oxymethylene ether-2 (OME_2) that, due to its high oxygen content and lack of direct carbon-carbon bonds, considerably reduces the formation of soot particles. To meet the challenges of a more flexible and sustainable power generation, a detailed understanding of its combustion properties is essential for its safe and efficient utilization, neat or in blends. In this work, two fundamental combustion properties of TMOF were studied: (i) Auto-ignition of TMOF / synthetic air mixtures (φ = 1.0; diluted 1:5 with N_2) using the shock tube method at pressures of 1, 4, and 16 bar, and (ii) Laminar burning velocities of TMOF / air mixtures using the cone angle method at ambient and elevated pressures of 3 and 6 bar. Furthermore, the impact of TMOF addition to a gasoline surrogate (PRF90) on ignition delay times was studied using the shock tube method at φ = 1.0, 1:5 dilution with N_2, T = 900-2000 K, and at 4 bar. The experimental data sets have been compared with predictions of the in-house chemical kinetic reaction mechanism (DLR Concise mechanism) developed for interpreting the high-temperature combustion of a broad

spectrum of different hydrocarbon fuels as well as oxygenated fuels, including TMOF. The results demonstrate that the ignition delay times of TMOF and OME_2 are nearly identical for all pressures studied in the moderate-to high-temperature region. The results obtained for the blend indicate that ignition delay times of the TMOF / PRF90 blend are shorter than those of the primary reference fuel 90 (PRF90) at 4 bar. In the lean-to stoichiometric region, the results obtained for laminar burning velocities of TMOF and OME_2 are similar. However, in the fuel-rich domain ($\varphi > 1.0$), laminar burning velocities for TMOF are noticeably lower, indicating a decreased reactivity. The model predictions based on the in-house model reveal a good agreement compared to the measured data within the experimental uncertainty ranges. In addition, sensitivity analyses regarding ignition delay times and laminar flame speeds were performed to better understand TMOF oxidation.

Keywords: biofuel, oxymethylene ether, laminar flame speed, ignition delay time, soot, primary reference fuel.

INTRODUCTION

As a response to the growing need to address environmental challenges caused by the combustion of fossil-based fuels and the depletion of fossil fuels, the production and adoption of unconventional fuels, ideally sustainable ones, in power generation, and transportation as well, has risen [1, 2]. Additionally, improvements in fuel flexibility are required to meet the sustainable energy production in the near future, notably in power generation, *i.e.*, in micro gas turbines and stationary gas turbines. However, a comprehensive knowledge about the combustion properties at the appropriate temperatures, pressures, and fuel-air ratio regimes is a prerequisite to ensure a safe and efficient operation. In this context, the use of oxygenated alternative fuels is considered as a promising way in order to meet strict future emission regulation norms while also reducing the dependency on fossil-based fuels.

Amongst the oxygenates, oxymethylene ethers (OME_n: $CH_3O(CH_2O)_nCH_3$, with n = 1-5) are receiving increased attention due to their strong potential in reducing soot and particulate emissions, particularly when used as diesel substitutes or additives [3-8]. OMEs can be produced from renewable resources through: (i) the power-to-liquid technology (PtL) [7, 9] or using biomass via gasification or sugar fermentation [10, 11]. Due to their high oxygen content, the application of OME_n in diesel engines has a positive impact on the classical trade-off between the control of soot/particulate matter and nitrogen oxides (NO_x). Further on, the deployment of OME_n is very appealing in conventional diesel engines with only modification of the sealing material [7, 12] due to their high cetane numbers, typically above 55 for OME_{2-5}, and high evaporation rates. Recently, researchers have begun to consider trimethyl

orthoformate (TMOF) as a potential biofuel [13]. TMOF is a branched isomer of oxymethylene ether-2 (OME_2) and thus, also has the potential to significantly reduce the formation of soot particles due to its high oxygen content and the absence of direct carbon-carbon bonds; see Fig. 1.

Research on the combustion of TMOF attracts researchers' interest because of its similarities to OMEs, implying that it may be useful as an alternative fuel. TMOF has been demonstrated to be an oxygenated fuel for direct oxidation in liquid-feed fuel cells [15-18]. With regard to their application in diesel engines and thus, also in gas turbines, Yeh *et al*. [13] demonstrated that blending TMOF into diesel reduces emissions. Recently, Gaiser *et al*. [14] measured the speciation data during oxidation of TMOF and OME_2 in an atmospheric flow reactor at φ-values of 0.8 and 1.2 for temperatures between 748 K and 1273 K. The results showed almost similar species pools that differed only in mole fractions. Hydrocarbon species such as C_2H_4, C_2H_6, and C_3H_6 were higher for TMOF. The additional methoxy group in TMOF lowers the C-H bond dissociation energy at the central carbon, so hydrogen abstraction at the central C-H is the primary pathway at lower temperatures. In another study, Döntgen and Heufer [19] have developed a detailed chemical kinetic model of TMOF based on the OME_1 model from Jacobs *et al*. [20]. For validation of their model, they measured ignition delay times of stoichiometric TMOF / air mixtures at pressures of 20 and 40 bar in the temperature range between 700-1000 K using the shock tube method. It was shown that unimolecular decomposition and H-atom abstraction by OH radicals are the dominant depletion channels. In addition, Döntgen *et al*. [21] investigated experimentally and theoretically the pyrolysis kinetics of TMOF and observed that the key consumption reaction is the methoxy-induced H-atom migration, which results in methanol. Further previous work on TMOF focused on H-atom abstraction by OH [22-24].

To this end, a detailed investigation of the fundamental combustion properties of TMOF, such as auto-ignition and laminar flame speeds, is required to evaluate their application potential and to develop safe and more advanced engines. Auto-ignition of TMOF has only been reported for elevated pressures of 20 and 40 bar and in the temperature region between 700 and 1000 K by Döntgen and Heufer [19]. For laminar burning velocities, no data are available in the literature. Thus, the purpose of this work is to investigate auto-ignition and laminar burning velocities of TMOF at conditions not considered before through a combined experimental and modeling method; see Table 1. The ignition delay times of stoichiometric mixtures of TMOF / synthetic air diluted 1:5 in N_2 were measured behind the reflected shock wave at pressures of 1, 4, and 16 bar and for temperatures between 900 and 1700 K. The laminar burning

velocities of TMOF / air mixtures have been determined by using a Bunsen burner and by applying the cone angle method at ambient (1 bar) and at elevated pressures of 3 and 6 bar for a preheat temperature of T = 473 K.

Also, since oxygenated fuels are discussed as promising additives or substitutes for conventional fossil-stemmed fuels, we reported herein the effect of the addition of TMOF to a gasoline surrogate, here the primary reference fuel 90 (PRF90: 90% *iso*-octane + 10% *n*-heptane, by liq. vol.), on ignition delay times. Ignition delay times of a blend (by liq. vol.) of 70% TMOF + 30% PRF90 / synthetic air at φ = 1.0, p = 4 bar, and a dilution of 1:5 with N_2 are measured; their results are compared to those of TMOF experimentally determined within this work and those of PRF90 obtained at similar conditions [25].

In addition, this work seeks to disentangle the reactivity of TMOF (also called *iso*-OME_2) from its linear isomer OME_2 with respect to combustion properties and thus, to establish the effect of their structural difference on IDTs and LBVs. Therefore, the results of the present work obtained for TMOF are compared to those of its linear isomer OME_2 obtained earlier in the same experimental facilities at similar conditions. The experimental data sets obtained were used for checking the performance of an in-house reaction model. In summary, the findings of the present work will contribute to a better understanding of TMOF combustion as well as to the design and optimization of burners and engines to be operated with this oxygenated renewable fuel.

The potential for power generation from OMEs including TMOF in gas turbines is an intriguing area that merits more consideration. So far, practically no information is available on their application in gas turbines. While utility-scale gas turbines are designed to run on natural gas with a premium liquid fuel like diesel or fuel oil as an alternate or backup fuel, micro gas turbines may run on a far broader spectrum of gaseous and liquid fuels. Previous research has shown that combustion of various oxygenated fuels such as ethanol, *iso*- and *n*-butanol, and methanol, either neat or co-firing with liquid and gaseous fuels, meet the requirements for use in micro gas turbines and stationary gas turbines [26-30]. It is worth to note that OMEs are superior to alcohols, with better cetane numbers and high oxygen content. Thus, their combustion, neat or co-firing with liquid fuels *e.g.,* diesel, gasoline or kerosene and gaseous fuels, such as *e.g.,* natural gas and biogenic gases would be viable options for achieving clean combustion in micro gas turbines. For utility gas turbines, neat OMEs or OME / diesel blends could make a good back up fuel and thus, contribute to reduction of soot particles, besides of NO_x emissions. However, the storage of OMEs with respect to

compatibility with materials and their long-term stability requires to be investigated. In addition, due to the notable differences in heating values (lower heating values) of OMEs (22.4 MJ/kg for OME_1, 17.7 MJ/kg for OME_4, and about 20.5 MJ/kg for TMOF) [6, 31] and classical gas turbine fuels (47.1 MJ/kg for natural gas and 42.6 MJ/kg for diesel) [32], the need for structural re-adjustments in the design of the specific gas turbine when using OMEs is foreseen, *i.e.,* of the nozzles and the combustion chamber. The results obtained in this work, particularly on laminar burning velocities and ignition delay times, are also enabling knowledge-based critical discussions and assessments on the safety of their use in gas turbines.

EXPERIMENTAL

To study the combustion properties of TMOF, ignition delay times and laminar burning velocities were measured. In this section, a detailed description is provided for the shock tube method of ignition delay time measurements and the cone angle method of laminar burning velocities measurement.

Measurement of ignition delay times

The experimental setup and its validation have already been described in detail in our previous work [33-36]. In summary, all ignition delay time measurements were conducted in a stainless-steel shock tube with a constant inner diameter of 9.82 cm (see Fig. 2). The double aluminum diaphragms separate the shock tube into a 5.8 m long driver section and a 11.35 m long driven section. To generate various shock wave strengths, diaphragms of varying thickness were utilized. Before each experiment, a vacuum pump system evacuates the shock tube to a pressure of less than 5.0×10^{-6} mbar. Tailored mixtures of helium and argon both with purity of 99.996% and 99.999%, respectively, were used as the driving gas in order to a achieve a tailored interface condition and so extend the observation period up to about 15 ms. The flow rates of helium and argon were controlled by two Bronkhorst mass flow controllers.

The combustible mixtures were prepared in a 128 L stainless-steel tank. The tank is evacuated to low pressures (below 5×10^{-6} mbar) by a turbomolecular pump. The temperature of the tank was adapted to 373 K to prevent the condensation of TMOF (*b.p.* = 373.8 K) in the combustible mixture. The fuel-oxidizer-diluent combinations were prepared following Dalton's law of additive pressures, as outlined in earlier publications [33, 37]. To ensure adequate mixing, the mixtures were left to settle overnight before the experiments started. Table 1 shows the detailed composition in parts per million (ppm) of the mixtures used in this investigation. The gases used were obtained from

Linde AG with the following purities: O_2 – 99.9999%, N_2 – 99.9999%, and synthetic air – 99.999%. TMOF was obtained from Alfa Aesar with a specified purity of > 99.00% by mass.

Due to the mixing and storage time at high temperatures necesary to avoid fuel condensation, degradation of the fuel in the combustible shock tube's mixtures was observed. As a consequence, using gas chromatography, the purity of each fuel-oxidizer-diluent combination was checked and monitored for thermal degradation products and residual compounds. The thermal breakdown products methyl formate (CH_3OCHO) and methanol were found and their levels were checked. Table 1A shows the average combined levels of TMOF, methyl formate, and methanol.

Ignition was monitored at the measurement plane located 10 mm from the end wall in two ways: (i) By measuring the pressure profile with a piezoelectric pressure transducer (Kistler 603B) which is shielded against signal drift due to flash temperature by at least a 1 mm layer of RTV106 silicon rubber, and (ii) by measuring the chemiluminescence signals of the excited CH* radicals observed at wavelengths of 431 nm. In addition, the emission signal of CH* at 431 nm was observed at the axial position (head-on) through the end plate window. The emissions were detected by a narrow band pass interference filter (Hugo Anders, FWHM = 5 nm) and measured with a photo-multiplier (type, HAMAMATSU R3896). The incident shock wave velocity was calculated using the time intervals recorded by the four pressure transducers mounted on the side wall at a constant spacing of 200 mm between the pressure transducers. The velocity of the shock at the end wall was obtained by extrapolating the axial velocity profile to the end wall. Finally, the pressure (p_{init}) and temperature (T_{init}) immediately behind the reflected shock wave were calculated based on a one-dimensional normal shock model with the measured incident shock velocity and velocity attenuation, initial temperature, mixture composition (see Table 1), and thermodynamic properties as input parameters.

The relative error in measuring the incident shock wave velocity for this shock tube series was determined to be less than 1%, which translates to errors of about ±10 K in initial temperature and ±1.8% in initial pressure behind the reflected shock wave.

Figure 3 shows, for the TMOF + PRF90 (70:30) / synthetic air / N_2 mixture, typical pressure and normalized emission signals undertaken at p_{init} = 3.8 bar and T_{init} = 960 K for the determination of ignition delay time. All ignition delay time values presented in this work have been determined from the time difference between the formation of a

reflected shock wave at the end wall ($t/s = 0$) and the occurrence of CH* emission peak detected from the radial port (side-on), and in some configurations through the end wall window (axial or head-on); see Fig. 3.

Due to the different speeds of the combustion wave and the reflected shock wave, the radially derived ignition delay times are delayed. For this reason, the radially derived ignition delay times are related to the measurements at the end wall through a blast wave correction procedure using deflagration velocity obtained from the highest temperature measurements in the series [41, 42]. This approach assumes that ignition always start at the end wall, where the high temperature and high-pressure conditions are triggered first by the reflected shock wave, and that emission must first propagate before it can be detected via the radial measuring port. At our experimental conditions, correction due to blast wave can be up to 20 µs. The significance of the blast wave correction error (on side wall data) reduces as temperature reduces. In our measurements, the level of dilution applied (1:5 with N_2) decreases the blast wave speed, and thus, also the discrepancy between the radial and axial data. Nevertheless, for extremely short ignition delay times, generally around and below 10 µs, the axially derived ignition delay time can be taken as an upper bound because the blast wave correction is not required for axial emission detection. The detection setup comparison of both emission signals (radial with axial) decreases the inaccuracy of ignition delay time measurements at the maximum temperatures to ±30%, despite the blast wave correction process being required for the radial port emission detection measurements [39].

In Fig. 3, the pressure profile is constant immediately behind the reflected shock wave, and then increases gradually up to 5200 µs due to post shock compression, *i.e.*, due to effects of viscous gas dynamics following the interaction of the reflected shock wave with the boundary layer formed behind the incident shock wave. For the condition of this experiment, the increase in pressure is more pronounced because of the extended observation period. The post shock compression reaches a maximum at 5200 µs, and after this, the pressure remains uniform and increases at the vicinity of ignition at about 7500 µs, due to heat release. Even in non-ignitable mixtures, pressure rise due to viscous gas dynamics cannot be prevented without taking further measures such as driver gas dynamic mass flow reduction induced by the use of driver inserts [43, 44].

To account only for the increase in pressure due to gas dynamics, a pressure profile $p = p\ (t)$ derived from measurements with long ignition delay times and from non-ignitable mixtures with similar acoustic impedance is

provided to the calculations. After the maximum compression, the pressure profile is extrapolated to constant level because the pressure should remain constant in a well-tailored case, see the dashed black line in Fig. 3. The CH* emission signal remains at zero level up to about 7000 µs and then rises steeply indicating ignition.

Measurement of laminar burning velocity

Laminar burning velocities (LBVs) measurements were carried out using a high-pressure burner that produces a conical flame. The measurements were performed for a TMOF / air mixture at a preheat temperature of 473 K and ambient (1 bar) and elevated pressures (3 and 6 bar) covering the equivalence ratio φ between 0.6 to 1.8. The experimental setup and the method of measurement are given in more detail in our previous work [36, 37, 45]. Thus, just a brief description is presented here.

The fuel TMOF was vaporized at 413 K (140 °C) at 1 bar with the flow rate controlled by an HPLC-pump (type LC-20AD, Shimadzu). The vaporization temperature was raised to 443 K (170 °C) and 493 K (220 °C), respectively at 3 and 6 bar. TMOF was vaporized and then diluted with a heated nitrogen-flow (N_2, Linde AG, 99.999%). The temperature of the TMOF-N_2 mixture was adjusted to 473 K, and preheated oxygen (O_2, Linde AG, 99.95%) was added. The flow rates of oxygen and nitrogen were set according to the composition of air, *i.e.*, N_2:O_2 = 79:21. The O_2 flow rate was controlled by a calibrated mass flow controller (MFC) (Bronkhorst High-Tech B.V., type F-111B) as it was the case for the N_2 flow at the 1 bar measurements, too. However, for the measurements at 3 bar and 6 bar, the N_2 flow was controlled using a coriolis mass flow meter (Bronkhorst High-Tech B.V., mini Cori-Flow type 12) in combination with a control valve (Vary-*P* type F-033).

The combustible mixtures were burnt at the outlet of a converging nozzle. In our experiments, a co-flow is employed to stabilized the flame over a wide range of fuel-air ratio. Air is used as co-flow in fuel-rich conditions ($\varphi \geq 1$), whereas a mixture of 5% CH_4 + 5% H_2 + 90% N_2 is used in fuel-lean conditions ($\varphi \leq 1.0$), as reported in our previous publication [37].

The laminar burning velocity S_u for each measurement condition is derived by using the cone angle method according to Eq. (1). The cone angle α is derived from the images of the conical shaped flames captured by a CCD-

camera (type Imager Intense, LaVision GmbH), and the velocity v_u of the unburned gas is determined from the measurement [36, 37, 45].

$$S_u = v_u \cdot \sin \alpha \qquad \text{(Eq. 1)}.$$

MODELING

In this work, a comparison is given between the measured data and modeling predictions using the detailed chemical kinetic in-house model (DLR Concise) by Kathrotia *et al*. [46]. This mechanism consists of 313 species taking part in 2148 reactions and was developed for the surrogate modeling of a wide spectrum of hydrocarbon fuels, which include jet fuels, diesel, and gasoline. It also covers the oxidation of various oxygenated species such as alcohols (C_1-C_4) and oxymethylene ethers (OME_n, n = 0-5). Incorporated in the mechanism is also a high-temperature sub-model for TMOF. To the best of our knowledge, the DLR Concise mechanism is presently the only publicly accessible model for TMOF oxidation. The mechanism has been extensively validated for about 70 neat hydrocarbon species over a wide range of experimental conditions*, i.e.*, shock tubes, jet-stirred reactors, flow reactors, and laminar flames.

Calculations of ignition delay times were performed using the Chemkin II package [47] based on the 0-dimensional homogeneous reactor model, with the composition of the mixture (see Table 1), initial temperature, and pressure behind the reflected shock wave. In addition, an experimental pressure profile of the form p_5 / p_5 (t = 0) was incorporated into the calculations to account for the time dependent pressure and temperature rise due to gas dynamic effects, and disregarding any pressure rise due to heat release. Cantera software was used to calculate laminar flame speeds for a freely propagating flame and employing multi-component and thermal diffusion models [48].

RESULTS AND DISCUSSION

In this section, the results of the measurements and predictions by the in-house reaction model (DLR Concise) from Kathrotia *et al.* [46] are presented and discussed. First, ignition delay times determined for N_2-diluted mixtures of TMOF / synthetic air, TMOF / PRF90 blend, and OME_2 / synthetic air are discussed. The second part focuses on laminar burning velocities of TMOF / air determined for p / bar = 1, 3, and 6.

Ignition delay times

Figure 4 shows the results of measured (symbols) versus predicted (curves) ignition delay times of TMOF / synthetic air mixtures obtained at φ = 1.0, a dilution level of 1:5 with N_2, and pressures of 1, 4, and 16 bar. The measurements were done in the intermediate to high temperature range between 830 and 2000 K, due to the high level of dilution applied (see Table 1). The measurements were made up to about 11 ms (see the dashed black line). The measured data exhibit a linear relationship with temperature up to about 1200 K depending on pressure indicating an Arrhenius behavior. At temperatures below 1200 K, the IDTs deviate slightly from linear behavior, becoming shorter mainly due to greater reactivity induced by viscous gas dynamics, *i.e.*, interaction of the reflected shock wave with the boundary layer left behind by the incident shock wave. This effect is well pronounced for elevated pressures of 4 and 16 bar. The experimental pressure profile is used to account for this tendency in modeling. The shown trend of IDTs decreasing with increasing pressure is expected. In terms of temperature and pressure, an ignition delay time correlation of the Arrhenius type was derived for each data series using regression analysis as described by Zhang *et al*. [49] and Hu *et al.* [50]. Using this correlation and based on temperature and pressure uncertainties, ignition delay time uncertainties of up to 30% on all measured values were observed. The closeness between the model predictions and the experimental data is observed for temperatures ranging from 1250 to 2000 K at p / bar = 1, 4 and 16 bar. The model also fails to account for IDT's pressure dependence at temperatures lower than 1250 K, notably for 1 and 16 bar. The discrepancy between measurements and model predictions, particularly at temperatures below 1250 K, is attributed to insufficient mechanism validation as well as an absence of low temperature chemistry.

TMOF is suggested as a carbon-reduced renewable biofuel that might possibly be blended with conventional gasoline to minimize soot emissions while simultaneously lowering combustion-related CO_2 emissions. The effect of introducing 70% TMOF (by liq. vol.) to a gasoline surrogate (PRF90) on ignition delay times was investigated in this study for a φ-value of 1.0 (stoichiometric), a dilution level of 1:5 with N_2, and a pressure of 4 bar. The primary reference fuel 90 (PRF90), a binary combination of 90% *iso*-octane and 10% *n*-heptane, was chosen as the gasoline surrogate since it has been proved to be an acceptable gasoline surrogate in terms of ignition and knocking [51, 52]. The results are presented in Fig. 5. They are compared to those obtained under comparable conditions for: (i) TMOF / synthetic air reported in this work; and (ii) PRF90 / synthetic air reported in our previous work [25]. The results demonstrate that the addition of TMOF shortened the IDTs over the entire temperature regime. This indicates that TMOF promotes the ignition of PRF90. The predictions with the in-house model are close to the measured data for

both the neat fuels and the binary fuel. TMOF, like oxymethylene ethers, enhances the reactivity of the system by increasing the radical accumulation during the ignition delay time period [25]. An increase in radical concentration implies that the system's reactivity has increased, and as such, the IDTs of the binary fuel become shorter.

Ignition delay time-sensitivity analyses

A sensitivity analysis was performed by perturbing the rates of each individual reaction to further examine the oxidation of TMOF at high temperatures identifying the important reactions governing the reactivity. Equation (2) defines the normalized sensitivity coefficient, where the superscript "ref" refers to the unperturbed system. Reactions with negative sensitivity promote ignition by increasing the reactivity, and vice versa.

$$S_i = (k_i^{ref} / \tau_i^{ref}) * \left[d\tau_{ign} / dk_i \right] \qquad \text{Eq. (2)}$$

The results for TMOF / synthetic air mixture at $\varphi = 1.0$, dilution level of 1:5 with N_2, $T = 1300$ K, and for pressures of 1, 4, and 16 bar are displayed in Fig. 6. The results show that, like most hydrocarbon fuels, the ignition of TMOF is very sensitive to the chain branching reaction $H+O_2 \Leftrightarrow O+OH$. The chemistry of small radicals dominates the ignition regime under the conditions examined; this was shown earlier for OME_1 and OME_2 in the intermediate to high temperature range [33, 40]. The system is also extremely sensitive to further chain branching reactions $HO_2+H \Leftrightarrow OH+OH$, $CH_3+HO_2 \Leftrightarrow CH_3O+OH$, and $HCO+M \Leftrightarrow HCO+H+M$. In Fig. 7, the results of the sensitivity analysis of the stoichiometric mixture of TMOF / synthetic air are presented at $p = 4$ bar for T / K= 1100, 1300, and 1600. The results are remarkably similar to those shown in Fig. 6. In general, it is observed that reactions involving the chemistry of small radicals are shown to be the dominant ones.

Laminar burning velocities

The results of the measured laminar burning velocities (LBV) as well as the calculated laminar flame speeds (LFS) of TMOF-air mixtures are presented in Fig. 8 for all three pressures studied – p / bar = 1, 3, and 6 – at the preheat temperature T / K = 473. The flames have been stabilized in a wide fuel-air ratio regime, of about $\varphi = 0.65$ and $\varphi = 1.8$, due to the co-flow applied.

For all pressures studied, the maximum LBVs are observed at $\varphi = 1.1$. At atmospheric pressure, a value for $S_u = 100$ cm/s was measured, and at elevated pressures, the experiments yielded LBV values of 78.4 cm/s ($p = 3$ bar)

and 65.6 cm/s (p = 6 bar), respectively. The uncertainties of the measurements were estimated using the law of error propagation, by considering the accuracies of pressure, temperature, and gas flow, as well as the deviation of the cone angle. The error analysis showed that the accuracy of the measurements is mostly influenced by pressure and fuel-air ratio. At 1 bar, the uncertainties are estimated to an average value of about ±2 cm/s corresponding to a relative error of ±2-4%. At elevated pressures, the uncertainties range from ±3% to ±10%, with up to ±15% for fuel-rich mixtures (φ > 1.4). The absolute values amount to ΔS_u = 2-5 cm/s at 3 bar and 3-7 cm/s at 6 bar. At these high fuel-air ratios, the uncertainties are mostly induced by difficulties in flame stability resulting in varying cone angles. As mentioned above, pressure fluctuations and the accuracies of the mass flow controllers have a further impact on the uncertainty.

The results of predictions using the DLR Concise model from Kathrotia *et al.* [46] show that the maximum LFSs are located at nearly the same position (φ = 1.10-1.15). The model shows an overprediction of about 5-6 cm/s over nearly the entire φ range studied and at all pressures investigated. However, at high pressures and φ > 1.50, the model underpredicts experimental data, presumably because due to higher errors in measurement at these conditions.

Laminar burning velocity-Sensitivity analyses

In Figs. 9 and 10, results of the sensitivity analyses are shown with a comparison of various φ-values at p = 1 bar (Fig. 9) and at φ = 1.2 for the three pressures investigated (Fig. 10). When compared to the results of the sensitivity analyses of IDT, here no fuel-specific reaction is observed for laminar flame speeds within the 15 most sensitive reactions.

At 1 bar, the accelerating reactions $H + O_2 \Leftrightarrow O + OH$ and $HCO + M \Leftrightarrow CO + H + M$ are most important for the oxidation process (see Fig. 9). Here, the sensitivity of the $H + O_2$ reaction increases with rising φ-values, whereas the sensitivity of the HCO consumption reaction reduces. The promoting effect of both reactions results from the formation of the most reactive, and thus, important radicals, O, OH, and H. The most inhibiting reactions involve consumption of H radicals to form stable products and less reactive species through: $CH_3 + H (+M) \Leftrightarrow CH_4 (+M)$ and $H + HCO \Leftrightarrow CO + H_2$.

The comparison of the sensitivities for the three pressures (1, 3, and 6 bar) at the φ-value (φ = 1.2) close to the peak value reveals that the $H + O_2$ reaction is the most important reaction promoting oxidation of TMOF oxidation,

see Fig. 10. At 6 bar, the sensitivity coefficients of a number of reactions are referred in reverse direction compared to 1 bar and 3 bar.

Comparison of combustion properties TMOF and OME_2

Due to its similarities to OME_2, this work also seeks to disentangle the structural differences between TMOF and its linear isomer OME_2 with respect to ignition and laminar burning velocities. As a result, the TMOF results in this study are compared to those of its linear isomer OME_2 produced previously in the same experimental facilities under identical conditions [33]. In Fig. 11, a comparison is given of the measured IDT data for TMOF / synthetic air and OME_2 / synthetic air for p / bar = 1 and 16. The results reveal that the IDTs of the two fuels are similar within experimental uncertainty. These results suggest that in the intermediate to high-temperature regime where the fuel rapidly pyrolyzes, the effect of structural difference on reactivity of the two ethers in negligible. The ignition delay times of TMOF are presented here for the first time for the intermediate to high temperature regime, and they provide an essential data set for further improvement of TMOF oxidation models.

To examine further the fuel specific differences with respect to ignition, the results of the sensitivity analysis for OME_2 and TMOF at 1200 K and p = 1 bar are presented in Fig. 12 (sorted according to TMOF). In both fuels, reactions involving the chemistry of small radicals are shown to be the dominant ones. However, it is observed that the ignition of TMOF is sensitive to reactions involving (i) Ethene: $C_2H_4 + H(+M) \Leftrightarrow C_2H_5(+M)$, and (ii) Methyl formate: $OCHOCH_3 + H \Leftrightarrow OCHOCH_2 + H_2$, $OCHOCH_3 + H \Leftrightarrow OCOCH_3+H_2$, and $OCHOCH_3 + OH \Leftrightarrow OCHOCH_2 + H_2O$. According to DLR Concise model, TMOF exclusively decomposes by the breaking of the C-O bond through TMOF $\Leftrightarrow O^*CH(OCH_3)_2+CH_3$ reaction. The primary fuel radical the radical $O^*CH(OCH_3)_2$ breaks down through β-scission forming methyl formate $OCHOCH_3$ and methoxy CH_3O radicals through $O^*CH(OCH_3)_2 = OCHOCH_3 + CH_3O$. Thus, methyl formate $OCHOCH_3$ is an important intermediate providing radical build-up, while for OMEs, formaldehyde CH_2O and HO_2 are the most important oxygenated species. This is in line with the work of Gaiser *et al*. [14], who measured higher mole fractions of hydrocarbons (C_2H_4, C_2H_6, and C_3H_6) as well as of the oxygenated species acetaldehyde (CH_3CHO) and methyl formate ($OCHOCH_3$) for TMOF compared to OME_2. Because the methyl (CH_3) radical is a precursor in the formation of hydrocarbon species, high hydrocarbon concentrations during TMOF oxidation can be attributed to high methyl concentration formed during the early stages of TMOF oxidation; for example, by the reaction TMOF $\Leftrightarrow O^*CH(OCH_3)_2 + CH_3$.

In Fig. 13, the experimental LBV and the calculated LFS data for TMOF and OME_2 [33] obtained at similar conditions are compared. DLR Concise model [46] matches exactly the experimental data for OME_2. Both the experiment and the modeling show that the maximum value for the LBVs of OME_2 are located at $\varphi = 1.2$. The experimental data shows that the LBVs of the two fuels are identical for fuel-lean mixtures, whereas at stoichiometric and fuel-rich conditions, the LBVs of OME_2 are distinctly higher by up to about 20 cm/s at $\varphi > 1.50$ and 1 bar.

Comparison of TMOF to alternative gas turbine fuels

The combustion behavior of TMOF in comparison to alternative gas turbine fuels is evaluated based on laminar burning velocities obtained at similar conditions, *i.e.*, at a preheat temperature of 473 K and at $p = 1$ bar. The results are shown in Fig. 14, where the laminar burning velocity values of TMOF from the present work are compared to those of *n*-butanol [36, 45], *iso*-butanol (unpublished), and a diesel surrogate [53]. The composition of the diesel surrogate is formulated to represent relevant diesel fuel properties and contains 50% n-dodecane + 30% farnesane (2,6,10-trimethyldodecane) + 20% 1-methyl-naphthalene (all mole percentages). These fuels were measured using the same experimental setup as for TMOF with the cone angle method applied for the determination of the LBVs.

The diesel surrogate has the lowest LBV, with a maximum of roughly 83 cm/s at = 1.1, as seen in Fig. 14. With maxima of 91 cm/s for *n*-butanol and 86 cm/s for *iso*-butanol, the LBVs of the C_4-alcohols are within those of TMOF ($S_{u,max}$ = 100 cm/s) and the diesel surrogate. Iso-butanol exhibits the lowest LBV only in very fuel-rich and fuel-lean mixtures; however, the differences are within the range of uncertainties. The highest LBV for TMOF indicates a higher reactivity, which is consistent with the results of the IDTs of TMOF and PRF90 presented before. Moreover, the general tendency demonstrated here is that the LBV and therefore the reactivity increases with the oxygen content of the fuel; this coincides with the findings from earlier studies that compared OME_1 with *n*-butanol and PRF90 [25, 40] and OME_4 with the diesel surrogate [53].

Furthermore, it is worth to mention the similarity in the results of OME_2 and TMOF compared to the data of *n*- and *iso*-butanol. Although there are no C-C bonds neither in OME_2 nor in TMOF, OME_2 shows the higher LBV as it is also the case for *n*-butanol compared to *iso*-butanol. The influence of a branched structure in fuel components to the combustion properties is known for pure hydrocarbon fuels [54] and, with the results found here, seems also of importance for oxygenated fuels.

SUMMARY AND CONCLUSIONS

In the current study, ignition delay times and laminar burning velocities of TMOF were investigated using a combined experimental and modeling approach. Ignition delay times of TMOF / synthetic air mixtures measured using the shock tube technique have been reported for the first time at φ = 1.0, dilution of 1:5 with N_2, pressures of 1, 4, and 16 bar and for temperatures ranging between 900-2000 K. The laminar burning velocities of TMOF / air mixtures determined using a Bunsen burner and applying the cone angle technique are reported for the first time at a preheat temperature T = 473 K and pressures of 1, 3, and 6 bar, for φ-values between 0.6-1.8. In addition, IDTs of a 70 % TMOF / 30 % PRF90 blend (by liq. vol.) determined using the shock tube method at: φ = 1.0, p = 4 bar, T = 950-2000 K, and a dilution of 1:5 with N_2. A comparison was presented between experimental and calculated data using the in-house DLR Concise model.

For ignition delay time, the in-house model replicates well the temperature and pressure dependence of IDTs of TMOF in the high-temperature regime between 1250-2000 K. However, the model fails to replicate the measured data for temperatures lower than 1250 K. For laminar burning velocities, the model overpredicts the measured LBV data for TMOF for the three pressures, with a maximum overprediction of up to 20 cm/s in the rich domain of the 1 bar series. The discrepancy between measured and calculated values is ascribed to insufficient mechanism validation as well as a lack of low temperature chemistry.

The ignition delay times of TMOF have been compared to those of its linear isomer OME_2 with the results showing nearly identical values in the intermediate to high-temperature regime. The values obtained for laminar burning velocities of TMOF and OME_2 are nearly similar. However, the laminar burning velocities of TMOF are lower in the fuel rich domain indicating a reduced reactivity. The TMOF / PRF90 blend reveals a higher reactivity when compared to PRF90 mixture. This enhanced reactivity was attributed to the addition of TMOF creating a higher radical build-up, thus accelerating the system. The results of sensitivity analyses of IDT and LBV calculations revealed that the chemistry of small radicals largely dominates the ignition regime.

This work is part of our ongoing efforts to characterize the combustion behavior of oxygenated fuels, alcohols, and notably ethers. The data obtained will allow for the improvement and optimization of TMOF reaction models, as well as facilitate critical discussion and assessment of the deployment of TMOF in (micro and remote) gas turbines.

Acknowledgments

We thank N. Ackermann for his help in the experimental setup. J.M.N. gratefully acknowledges financial support from the National Research Fund of Kenya and the German Academic Exchange Service (Funding Programme No: 57399475).

Nomenclature

p	Pressure [bar]
t	Time [s]
S_u	Laminar flame speed [cm/s]
S_i	Sensitivity coefficient []
v	Velocity of gas mixture [m/s]

Greek letters

α	Cone angle
λ	Wavelength
φ	Fuel equivalence ratio
τ	Ignition delay time
ρ	Density

Subscripts

init	Initial status behind reflected shock wave
l	Laminar
ign	Ignition
u	Unburnt

Abbreviations

OME	Oxymethylene ether
TMOF	Trimethyl orthoformate (*iso*-OME_2)
LBV	Laminar burning velocity
LFS	Laminar flame speed
PRF	Primary reference fuel
IDT	Ignition delay time

References

[1] Emberger, G., 2017: "*Low carbon transport strategy in Europe: A critical review*", Int. J. Sustain. Transp. 11(1), 31-35.

[2] European Commission, 2012: "*Commission Regulation (EU) No 459/2012 of 29 May 2012 amending Regulation (EC) No 715/2007 of the European Parliament and of the Council and Commission Regulation (EC) No 692/2008 as regards emissions from light passenger and commercial vehicles (Euro 6)(1)*".

[3] Hank, C., Lazar, L., Mantei, F., Ouda, M., White, R.J., Smolinka, T., Schaadt, A., Hebling, C., Henning, H.-M., Fuels, 2019: "*Comparative well-to-wheel life cycle assessment of OME_{3-5} synfuel production via the power-to-liquid pathway*", Sustain. Energy Fuels 3(11), 3219-3233.

[4] Kohse-Höinghaus, K., 2021: "*Combustion in the future: The importance of chemistry",* Proc. Combust. Inst. 38(1), 1-56.

[5] Liu, H., Wang, Z., Li, Y., Zheng, Y., He, T., Wang, J., 2019: "*Recent progress in the application in compression ignition engines and the synthesis technologies of polyoxymethylene dimethyl ethers*", Appl. Energy (233), 599-611.

[6] Liu, H., Wang, Z., Wang, J., He, X., Zheng, Y., Tang, Q., Wang, J., 2015: "P*erformance, combustion and emission characteristics of a diesel engine fueled with polyoxymethylene dimethyl ethers ($PODE_{3-4}$)/diesel blends*", Energy (88), 793-800.

[7] Omari, A., Heuser, B., Pischinger, S., Rüdinger, C., 2019: "*Potential of long-chain oxymethylene ether and oxymethylene ether-diesel blends for ultra-low emission engines*,", Appl. Energy (239), 1242-1249.

[8] Duan, X., Jia, M., Bai, J., Li, Y., 2021: "*Potential of reactivity-controlled compression ignition with reverse reactivity stratification (R-RCCI) fueled with gasoline and polyoxymethylene dimethyl ethers (PODE$_n$)*", Int. J. Engine Res., 14680874211013667.

[9] Deutz, S., Bongartz, D., Heuser, B., Kätelhön, A., Langenhorst, L. S., Omari, A., Walters, M., Klankermayer, J., Leitner, W., Mitsos, A., 2018: "*Cleaner production of cleaner fuels: wind-to-wheel–environmental assessment of CO_2-based oxymethylene ether as a drop-in fuel*", Energy Environ. Sci. 11(2), 331-343.

[10] Burger, J., Siegert, M., Ströfer, E., Hasse, H., 2010: "*Poly (oxymethylene) dimethyl ethers as components of tailored diesel fuel: Properties, synthesis and purification concepts*", Fuel 89(11), 3315-3319.

[11] Schmitz, N., Burger, J., Ströfer, E., Hasse, H., 2016: "*From methanol to the oxygenated diesel fuel poly (oxymethylene) dimethyl ether: An assessment of the production cost*", Fuel (185), 67-72.

[12] Pélerin, D., Gaukel, K., Härtl, M., Jacob, E., Wachtmeister, G., 2020: "*Potentials to simplify the engine system using the alternative diesel fuels oxymethylene ether OME_1 and OME_{3-6} on a heavy-duty engine*", Fuel (259), 116231.

[13] Yeh, L., Rickeard, D., Duff, J., Bateman, J., Schlosberg, R., Caers, R., 2001: "*Oxygenates: An evaluation of their effects on diesel emissions*", SAE Trans, 1482-1498.

[14] Gaiser, N., Bierkandt, T., Zinsmeister, J., Hemberger, P., Shaqiri, S., Kasper, T., Köhler, M., Aigner, M., 2021: "*Disentangling of linear and branched ethers: Flow reactor study of OME_2 and trimethoxy methane using molecular beam mass spectrometry and synchrotron photoionization*", Proc. 10th European Combust. Meeting.

[15] Chetty, R., Scott, K., 2007: "*Dimethoxymethane and trimethoxymethane as alternative fuels for fuel cells*", J. Power Sources 173(1), 166-171.

[16] Prakash, G.K.S., Smart, M.C., Olah, G.A., Narayanan, S.R., Chun, W., Surampudi, S., Halpert, G. 2007: "*Performance of Dimethoxymethane and Trimethoxymethane in Liquid-Feed Direct Oxidation Fuel Cells*", J. Power Sources, 173(1), 102-109.

[17] Wang, J.T., Lin, W.F., Weber, M., Wasmus, S., Savinell, R.F., 1998: "*Trimethoxymethane as an Alternative Fuel for a Direct Oxidation PBI Polymer Electrolyte Fuel Cell*". Electrochim. Acta, 43(24), 3821-3828.

[18] Narayanan, S.R., Vamos, E., Surampudi, S., Frank, H., Halpert, G., Surya Prakash, G.K., Smart, M.C., Knieler, R., Olah, G.A., Kosek, J., Cropley, C., 1997: "*Direct Electro-oxidation of Dimethoxymethane, Trimethoxymethane, and Trioxane and Their Application in Fuel Cells*", J. Electrochem. Society 144(12), 4195-4201.

[19] Döntgen, M. and Heufer, K.A., 2021: "*Shock Tube Study and Chemical Kinetic Modeling of Trimethoxymethane Combustion*", 10th Proc. European Combust. Meeting.

[20] Jacobs, S., Döntgen, M., Alquaity, A.B., Kopp, W.A., Kröger, L.C., Burke, U., Pitsch, H., Leonhard, K., Curran, H.J., Heufer, K.A., 2019: "*Detailed kinetic modeling of dimethoxymethane. Part II: Experimental and theoretical study of the kinetics and reaction mechanism*", Combust. Flam. (205), 522-533.

[21] Döntgen, M., Fuller, M. E., Peukert, S., Nativel, D., Schulz, C., Heufer, K. A., Goldsmith, C. F., 2022: " *Shock tube study of the pyrolysis kinetics of Di-and trimethoxy methane*", Combust. and Flam. (242), 112186.

[22] Platz, J., Sehested, J., Nielsen, O., Wallington, T., 1999: "*Atmospheric chemistry of trimethoxymethane, $(CH_3O)_3CH$; Laboratory studies*", J. Phys. Chem. A. 103(15), 2632-2640.

[23] Potter, D.G., Wiseman, S., Blitz, M.A., Seakins, P.W., 2018: "*Laser Photolysis Kinetic Study of OH Radical Reactions with Methyl tert-Butyl Ether and Trimethyl Orthoformate under Conditions Relevant to Low Temperature Combustion: Measurements of Rate Coefficients and OH Recycling*", J. Phys. Chem. A. 122(50), 9701-9711.

[24] Du, B. and Zhang, W., 2019: "*Theoretical study of the reaction mechanism and kinetics of the OH+ trimethyl orthoformate ($(CH_3O)_3CH$)+ O_2 reaction*", Comput. Theor. Chem. (1159), 38-45.

[25] Ngũgĩ, J. M., Richter, S., Braun-Unkhoff, M., Naumann, C., Riedel, U., 2022: "*A study on fundamental combustion properties of oxymethylene ether-1, the primary reference fuel 90, and their blend: experiments and modeling*", Combust. Flam., 111996, *in press,* available online: https://doi.org/10.1016/j.combustflame.2022.111996.

[26] Mendez, C.J., Parthasarathy, R.N., Gollahalli, S.R., 2014: "*Performance and emission characteristics of butanol/Jet A blends in a gas turbine engine*", Appl. Energy 118, 135-140.

[27] Chudnovsky, B., Reshef, M., Talanker, A., 2017: "*Evaluation of methanol and light fuel oil blends firing at a 50 MW gas turbine*", Proc. ASME Turbo Expo, GT-2019-57601.

[28] Glaude, P.A., Fournet, R., Bounaceur, R., Moliere, M., 2011: "*DME as a potential alternative fuel for gas turbines: A numerical approach to combustion and oxidation kinetics*", Proc. ASME Turbo Expo, GT-54617.

[29] Habib, Z., Parthasarathy, R., Gollahalli, S., 2010: "*Performance and emission characteristics of biofuel in a small-scale gas turbine engine*", Appl. Energy 87(5), 1701-1709.

[30] Klassen, M., Ramotowski, M., Eskin, L., Roby, R., 2010: "*Clean Combustion of liquid biofuels in gas turbines for renewable power generation*", AICE, LPP Combustion LLC, San Antonio, U.S.A., 1-6.

[31] Harnisch, F., Blei, I., dos Santos, T.R., Möller, M., Nilges, P., Eilts, P., Schröder, U., 2013: " *From the test-tube to the test-engine: assessing the suitability of prospective liquid biofuel compounds*", RSC advances, *3*(25), 9594-9605.

[32] Staffell, I., 2011: "*The energy and fuel data sheet*", *University of Birmingham*", accessed 2022-Feb-23, https://www.claverton-energy.com/wordpress/wp-content/uploads/2012/08/the_energy_and_fuel_data_sheet1.pdf

[33] Ngugi, J.M., Richter, S., Braun-Unkhoff, M., Naumann, C., Köhler, M., Riedel, U., 2022: "*A study on fundamental combustion properties of oxymethylene Ether-2",* J. Eng. Gas Turb. Power 144(1) 011014

[34] Braun-Unkhoff, M., Dembowski, J., Herzler, J., Karle, J., Naumann, C., Riedel, U., 2015: "*Alternative fuels based on biomass: An experimental and modeling study of ethanol cofiring to natural gas*", J. Eng. Gas Turb. Power 137(9).

[35] Herzler, J. and Naumann, C., 2008: "*Shock tube study of the ignition of lean CO/H_2 fuel blends at intermediate temperatures and high pressure*", Combust. Sci. Technol. 180(10-11), 2015-2028.

[36] Methling, T., Richter, S., Kathrotia, T., Braun-Unkhoff, M., Naumann, C., Riedel, U., 2018: "*An investigation of combustion properties of butanol and its potential for power generation*", J. Eng. Gas Turb. Power 140(9).

[37] Richter, S., Kathrotia, T., Naumann, C., Kick, T., Slavinskaya, N., Braun-Unkhoff, M., Riedel, U., 2018, "*Experimental and modeling study of farnesane*", Fuel (215), 22-29.

[38] Herzler, J., Herbst, J., Kick, T., Naumann, C., Braun-Unkhoff, M., Riedel, U., 2013: "*Alternative fuels based on biomass: An investigation of combustion properties of product gases*", J. Eng. Gas Turb. Power 135(3).

[39] Naumann, C., Janzer, C., Riedel, U., 2019: "*Ethane/nitrous oxide mixtures as a green propellant to substitute hydrazine: validation of reaction mechanism*", Proc. Europ. Combust. Meeting, Lisbon, Portugal, 14-17.

[40] Ngugi, J. M., Richter, S., Braun-Unkhoff, M., Naumann, C., Riedel, U., 2020: "*An investigation of fundamental combustion properties of the oxygenated fuels DME and OME_1*", Proc. ASME Turbo Expo, GT2020-14702.

[41] Petersen, E.L., 1999: "*A shock tube and diagnostics for chemistry measurements at elevated pressures with application to methane ignition*", PhD, Stanford University (USA).

[42] Petersen, E.L., 2009: "*Interpreting endwall and sidewall measurements in shock-tube ignition studies*", Combust. Sci. Technol. 181(9), 1123-1144.

[43] Hong, Z., Davidson, D.F., Hanson, R.K., 2009: "*Contact surface tailoring condition for shock tubes with different driver and driven section diameters*", Shock Waves 19(4), 331-336.

[44] Hong, Z., Pang, G.A., Vasu, S.S., Davidson, D.F., Hanson, R.K., 2009: "*The use of driver inserts to reduce non-ideal pressure variations behind reflected shock waves*", Shock Waves 19(2), 113-123.

[45] Richter, S., Braun-Unkhoff, M., Herzler, J., Methling, T., Naumann, C., Riedel, U., 2019: "*An investigation of combustion properties of a gasoline primary reference fuel surrogate blended with butanol*", Proc. ASME Turbo Expo. 2019, GT2019-90911.

[46] Kathrotia, T., Oßwald, P., Naumann, C., Richter, S., Köhler, M., 2021: "*Combustion kinetics of alternative jet fuels, Part-II: Reaction model for fuel surrogate*", Fuel 302(15), 120736, https://www.dlr.de/vt/mechanisms.

[47] Lutz, A.E., Kee, R.J., Miller, J.A., 1988: "*SENKIN: A FORTRAN program for predicting homogeneous gas phase chemical kinetics with sensitivity analysis*", Sandia National Labs., Livermore, CA (USA).

[48] Goodwin, D.G., Speth, R.L., Moffat, H.K., Weber, B.W., 2021: "*Cantera: An Object-oriented Software Toolkit for Chemical Kinetics, Thermodynamics, and Transport Processes*", https://www.cantera.org.

[49] Hu E., Gao Z., Liu Y., Yin G., Huang Z., 2017: "*Experimental and modeling study on ignition delay times of dimethoxy methane/n-heptane blends*", Fuel (189), 350-357.

[50] Zhang, Z., Hu, E., Pan, L., Chen, Y., Gong, J., Huang, Z., 2014: "*Shock-tube measurements and kinetic modeling study of methyl propanoate ignition*", Energy & Fuels 28(11), 7194-7202.

[51] Ra, Y. and Reitz, R.D., 2008: "*A reduced chemical kinetic model for IC engine combustion simulations with primary reference fuels*", Combust. Flam. 155(4), 713-738.

[52] Selim, H., Mohamed, S.Y., Hansen, N., Sarathy, S.M., 2017: "*Premixed flame chemistry of a gasoline primary reference fuel surrogate*", Combust. Flam. (179), 300-311.

[53] Richter, S., Kathrotia, T., Braun-Unkhoff, M., Naumann, C., Köhler, M., 2021: "*Influence of Oxymethylene Ethers (OME_n) in Mixtures with a Diesel Surrogate*", Energies (14), 7848.

[54] Kathrotia, T., Richter, S., Naumann, C., Slavinskaya, N., Methling, T., Braun-Unkhoff, M., Riedel, U., 2019: "*Reaction model development for synthetic jet fuels – Surrogate fuels as a flexible tool to predict their performance*", Proc. ASME Turbo Expo. 2018, GT2018-76997.

LIST OF FIGURE CAPTIONS

Fig. 1 Molecular structures of TMOF (also called *iso*-OME_2) and OME_2.

Fig. 2 Schematic diagram of the shock tube. The measurement plane is located 10 mm from the end wall [38-40]

Fig. 3 Typical pressure and emission signals for the determination of ignition delay time.

Fig. 4 Comparison of measured (symbols) and simulated (curves) IDTs (τ_{ign}) of TMOF / synthetic air mixtures diluted 1:5 with N_2 for φ = 1.0, p_{init} / bar = 1, 4, and 16 using $p = p(t)$. DLR Concise model used [46].

Fig. 5 Comparison of measured (symbols) and predicted (curves) IDTs (τ_{ign}) of synthetic air mixtures of TMOF, 70% TMOF + 30% PRF90, and PRF90 diluted 1:5 with N_2 at φ = 1.0, initial pressure of 4 bar using $p = p(t)$. DLR Concise model by Kathrotia *et al.* used [46].

Fig. 6 Sensitivity of ignition delay time of a stoichiometric mixture of TMOF / synthetic air calculated for p / bar = 1, 4, and 16 at T = 1300 K using the DLR Concise model by Kathrotia *et al.* [46].

Fig. 7 Sensitivity of ignition delay time of a stoichiometric mixture of TMOF / synthetic air calculated for T / K= 1100, 1300, and 1600 bar at p = 4 bar using the DLR Concise model by Kathrotia *et al.* [46].

Fig. 8 Measured laminar burning velocities of TMOF-air mixtures (symbols) and laminar flame speeds (curves) calculated using the DLR Concise model by Kathrotia *et al*. [46].

Fig. 9 Sensitivity of laminar flame speeds for three different TMOF-air mixtures calculated for p = 1 bar and T = 473 K using the DLR Concise model [46].

Fig. 10 Sensitivity of laminar flame speeds for TMOF-air mixtures calculated at $\varphi = 1.2$ for p = 1, 3, and 6 bar at T = 473 K using the DLR Concise model [46].

Fig. 11 Comparison of measured IDTs (τ_{ign}) of synthetic air mixtures of TMOF (*p.w.*) and OME_2 at initial pressures p / bar = 1 and 16, diluted 1:5 with N_2.

Fig. 12 Sensitivity of ignition delay time of stoichiometric mixtures of TMOF / synthetic air and OME_2 / synthetic air presented for T = 1200 K and p =1 bar using the DLR Concise model from Kathrotia *et al.* [46].

Fig. 13 Comparison of measured laminar burning velocities (symbols) and laminar flame speeds (curves) of TMOF-air mixtures (*p.w.*) and OME_2-air mixtures [33].

Fig. 14 Comparison of laminar burning velocities of TMOF-air mixtures (*p.w.)* to those of *n*-butanol [36, 45], *iso*-butanol, and a diesel surrogate [53].

LIST OF TABLE CAPTIONS

TABLE 1: Fuel-air mixtures studied in present work (*p.w.*).

Mixture	**Parameter range**		
	Fuel-air ratio φ	p / bar	T / K
A. Ignition delay time; dilution 1:5 with N_2. Composition given in ppm			
TMOF / synthetic air	1.0	1	1000-2000
7315 TMOF		4	900-2000
1214 CH_3OCHO		16	820-1700
664 CH_3OH			
38370 O_2			
952438 N_2			
70% TMOF + 30% PRF90 / synthetic air	1.0	4	900-2000
3358 TMOF			
299 CH_3OCHO			
494 CH3OH			
1601 *iso*-C_8H_{18}			
178 *n*-C_7H_{16}			
38799 O_2			
955270 N_2			
B. Burning velocity: Preheat temperature T_{preh} = 473 K. Composition given in molar fraction for φ = 1.0			
TMOF / air (21% O_2 + 79% N_2)	0.6 – 1.8	1	473
0.0403 TMOF + 0.2015 O_2 + 0.7582 N_2	0.6 – 1.8	3	473
	0.7 – 1.7	6	473

PRF90: 90% *iso*-octane + 10% *n*-heptane by liquid volume; synthetic air: 20% O_2 + 80% N_2; Dilution ratio of 1:5 means 20% fuel-air mixture + 80% N_2 by molar fractions

Figures

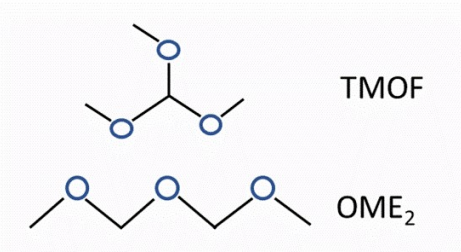

FIGURE 1: Molecular structures of TMOF (also called *iso*-OME_2) and OME_2.

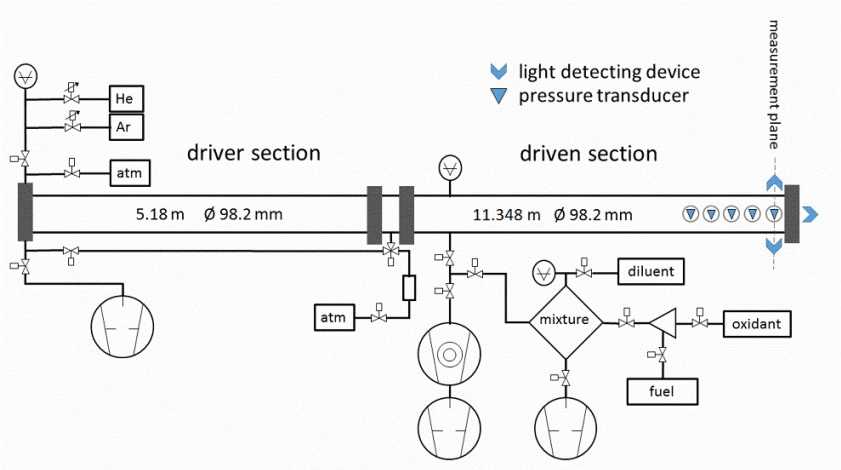

FIGURE 2: Schematic diagram of the shock tube. The measurement plane is located 10 mm from the end wall [38-40].

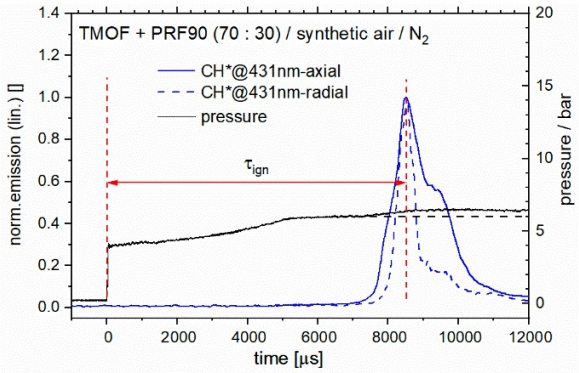

FIGURE 3: Typical pressure and emission signals for the determination of ignition delay time.

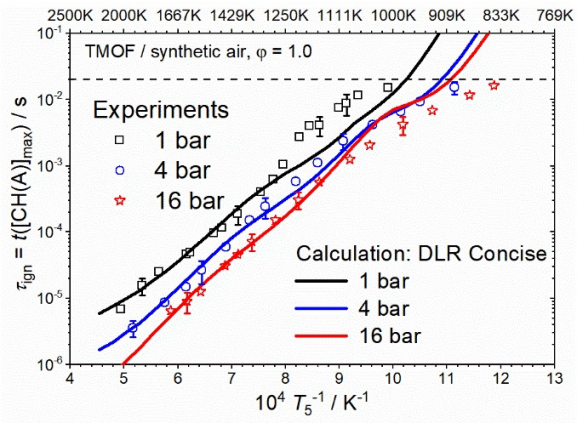

FIGURE 4: Comparison of measured (symbols) and simulated (curves) IDTs (τ_{ign}) of TMOF / synthetic air mixtures diluted 1:5 with N_2 for φ = 1.0, p_{init} / bar = 1, 4, and 16 using $p = p(t)$. DLR Concise model used [46].

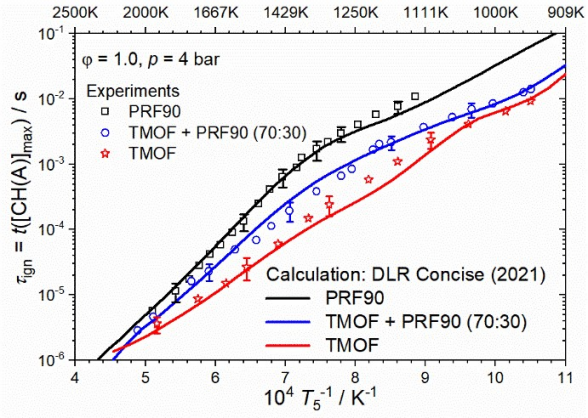

FIGURE 5: Comparison of measured (symbols) and predicted (curves) IDTs (τ_{ign}) of synthetic air mixtures of TMOF, 70% TMOF + 30% PRF90, and PRF90 diluted 1:5 with N_2 at φ = 1.0, initial pressure of 4 bar using $p = p(t)$. DLR Concise model by Kathrotia *et al.* used [46].

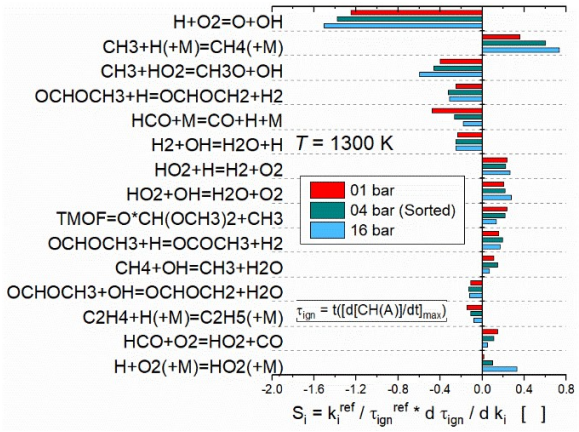

FIGURE 6: Sensitivity of ignition delay time of a stoichiometric mixture of TMOF / synthetic air calculated for p / bar = 1, 4, and 16 at T = 1300 K using the DLR Concise model by Kathrotia *et al.* [46].

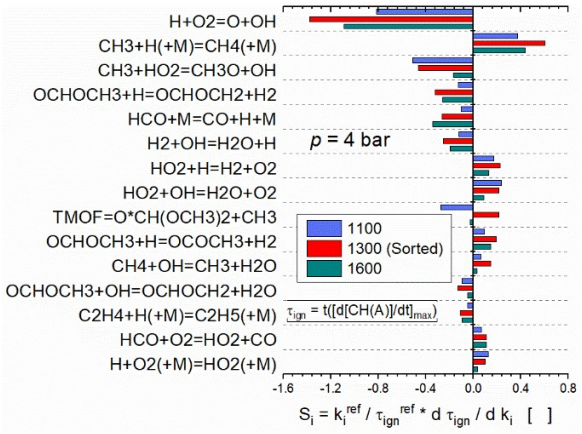

FIGURE 7: Sensitivity of ignition delay time of a stoichiometric mixture of TMOF / synthetic air calculated for T / K= 1100, 1300, and 1600 bar at p = 4 bar using the DLR Concise model by Kathrotia *et al.* [46].

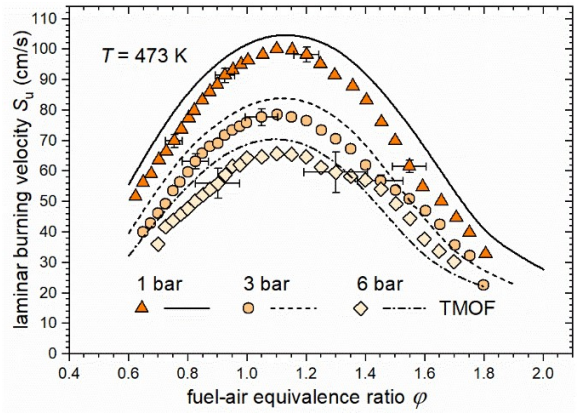

FIGURE 8: Measured laminar burning velocities of TMOF-air mixtures (symbols) and laminar flame speeds (curves) calculated using the DLR Concise model by Kathrotia *et al*. [46].

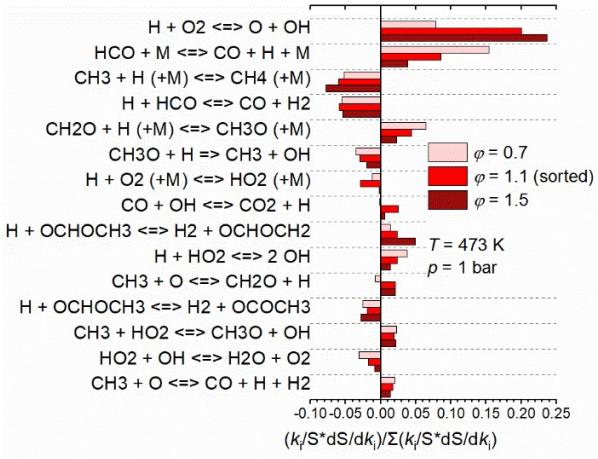

FIGURE 9: Sensitivity of laminar flame speeds for three different TMOF-air mixtures calculated for p = 1 bar and T = 473 K using the DLR Concise model [46].

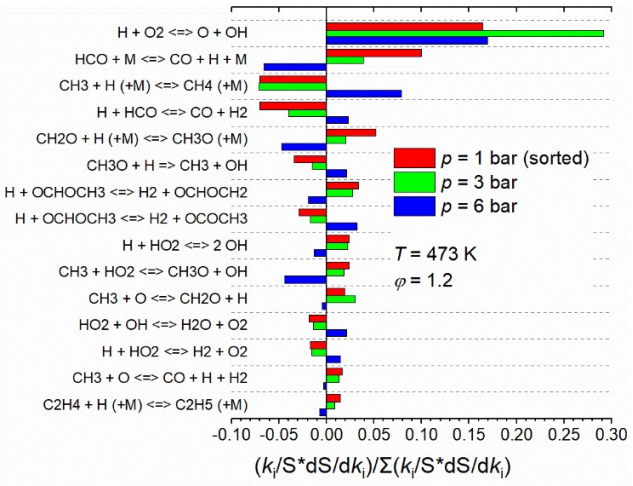

FIGURE 10: Sensitivity of laminar flame speeds for TMOF-air mixtures calculated at $\varphi = 1.2$ for $p = 1$, 3, and 6 bar at $T = 473$ K using the DLR Concise model [46].

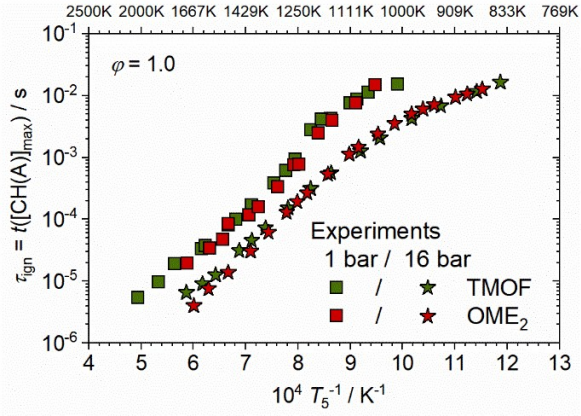

FIGURE 11: Comparison of measured IDTs (τ_{ign}) of synthetic air mixtures of TMOF (*p.w.*) and OME_2 at initial pressures p / bar = 1 and 16, diluted 1:5 with N_2.

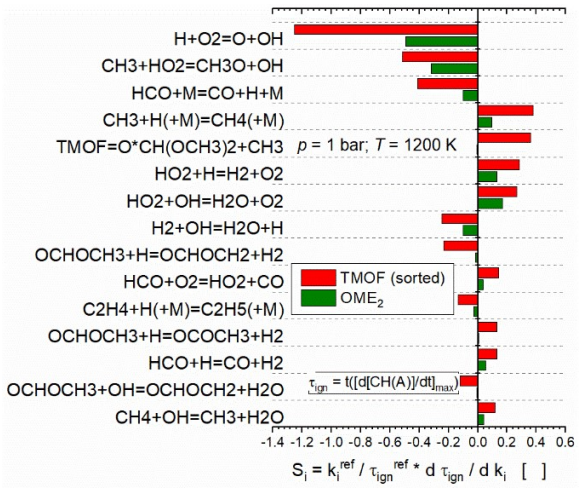

FIGURE 12: Sensitivity of ignition delay time of stoichiometric mixtures of TMOF / synthetic air and OME_2 / synthetic air presented for T = 1200 K and p =1 bar using the DLR Concise model from Kathrotia *et al.* [46].

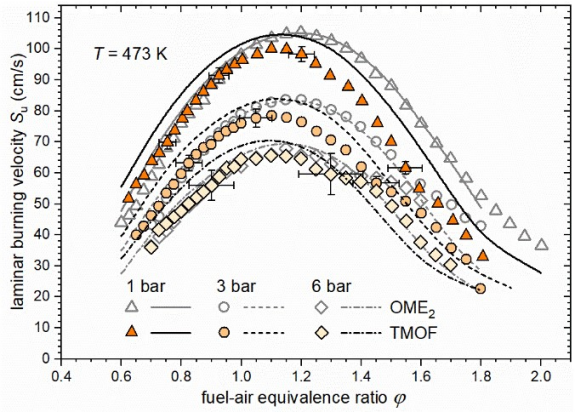

FIGURE 13: Comparison of measured laminar burning velocities (symbols) and laminar flame speeds (curves) of TMOF-air mixtures (*p.w.*) and OME_2-air mixtures [33].

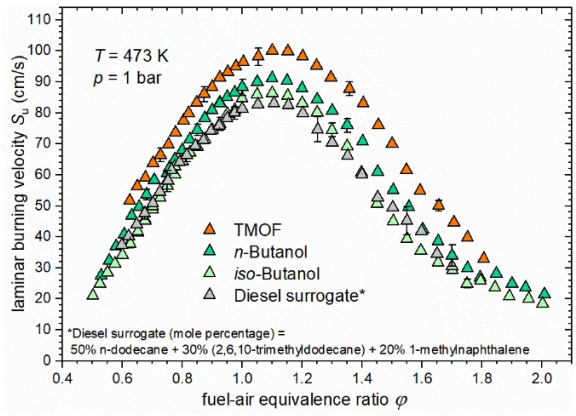

FIGURE 14: Comparison of laminar burning velocities of TMOF-air mixtures (*p.w.)* to those of *n*-butanol [36, 45], *iso*-butanol, and a diesel surrogate [53].